Cell Reports
Article

Generation of Regionally Specified Neural Progenitors and Functional Neurons from Human Embryonic Stem Cells under Defined Conditions

Agnete Kirkeby,[1,2,4] Shane Grealish,[1,4] Daniel A. Wolf,[1,2] Jenny Nelander,[1,2] James Wood,[2,3] Martin Lundblad,[1] Olle Lindvall,[2,3] and Malin Parmar[1,2,*]
[1]Department of Experimental Medical Science
[2]Lund Stem Cell Center
[3]Department of Clinical Sciences
Lund University, SE-221 84 Lund, Sweden
[4]These authors contributed equally to this work
*Correspondence: malin.parmar@med.lu.se
DOI 10.1016/j.celrep.2012.04.009

SUMMARY

To model human neural-cell-fate specification and to provide cells for regenerative therapies, we have developed a method to generate human neural progenitors and neurons from human embryonic stem cells, which recapitulates human fetal brain development. Through the addition of a small molecule that activates canonical WNT signaling, we induced rapid and efficient dose-dependent specification of regionally defined neural progenitors ranging from telencephalic forebrain to posterior hindbrain fates. Ten days after initiation of differentiation, the progenitors could be transplanted to the adult rat striatum, where they formed neuron-rich and tumor-free grafts with maintained regional specification. Cells patterned toward a ventral midbrain (VM) identity generated a high proportion of authentic dopaminergic neurons after transplantation. The dopamine neurons showed morphology, projection pattern, and protein expression identical to that of human fetal VM cells grafted in parallel. VM-patterned but not forebrain-patterned neurons released dopamine and reversed motor deficits in an animal model of Parkinson's disease.

INTRODUCTION

The successful derivation of human embryonic stem cells (hESCs) (Thomson et al., 1998) provided a new model system for studying human neural development, cell fate commitment, and neural disease mechanisms (Gaspard and Vanderhaeghen, 2011) and has opened up new strategies for regenerative medicine (Koch et al., 2009a). However, hESC neuralization protocols can be capricious, require extended in vitro culturing, and often depend on exogenous gene delivery as well as the use of feeder cells or other undefined components in the media, which limits their use as model systems and as donor cells for transplantation. Recent advances in hESC differentiation and lineage commitment have resulted in improved differentiation protocols for more efficient and synchronized neuralization of hESCs via dual inhibition of SMAD signaling (Chambers et al., 2009; Fasano et al., 2010). These protocols reduce the complexity of neural differentiation as they eliminate the need for feeder cells. However, they still require the use of undefined ingredients and animal-derived components (matrigel and knockout serum replacement [KSR]), which contain unknown components that can affect cell phenotype. KSR and matrigel are also subject to batch-to-batch variations, further hampering clinical translation (Ahrlund-Richter et al., 2009; Baker, 2011). In addition, the full range of neural progenitors that can be obtained using dual SMAD inhibition has not been determined and only one study to date shows transplantation data of neural progenitors obtained via dual SMAD inhibition (Kriks et al., 2011).

Here, we report a defined protocol for efficient generation of subtype-specific and regionalized neurons from hESCs based on dual SMAD inhibition and embryoid body (EB) formation (Chambers et al., 2009; Nat et al., 2007). By adding a chemical inhibitor of glycogen synthase kinase 3 (GSK3), we were able to induce dose-dependent activation of WNT signaling and control the positional specification of the cells so that distinct progenitors, with gene expression profiles matching neural progenitors from developing human fetal brain, ranging from telencephalic forebrain to rostral hindbrain fates, could be obtained. The positionally specified progenitors survived transplantation into the adult rat brain and formed neuron-rich grafts with maintained regional identity after only 10 days of differentiation in vitro. When combined with a high-potency form of sonic hedgehog (SHH-C24II), we could efficiently pattern the cultures toward a ventral mesencephalic (VM) fate, yielding a high number of floor plate progenitors that generated authentic and functional mesencephalic dopamine (mesDA) neurons comparable to that obtained from human fetal VM cells upon transplantation into an animal model of Parkinson's disease (PD).

RESULTS

Rapid and Efficient Neural Differentiation of hESCs Generated Progenitors with Telencephalic Gene Expression

We developed a neural differentiation protocol for hESCs by combining dual SMAD inhibition with EB formation (Chambers et al., 2009; Nat et al., 2007), thereby obtaining a culture setting of chemically defined reagents free of serum, KSR, and matrigel and devoid of any manual picking steps (Figure 1A). EBs were cultured in the presence of SB431542 and noggin for neural induction and the cell clusters were dissociated to single cells on day 11 for terminal differentiation (Figures 1A and 1B). The protocol resulted in rapid and complete downregulation of the pluripotency-associated genes, *OCT4* and *NANOG,* followed by induction of the neuronal markers *MAP2* and *SYP* (Synaptophysin) (Figure 1D). To induce mature neuronal morphologies, either dibutyryl-cAMP (db-cAMP) or the notch inhibitor N-[N-(3,5-Difluorophenacetyl)-L-alanyl]-S-phenylglycine t-butyl ester (DAPT) needed to be added to the medium from d14 (Figure 1C). Quantifications after 21 days of differentiation showed that over 80% of the cells were MAP2 positive under these conditions (84.1% ± 4.5% in db-cAMP and 87.2% ± 1.0% in DAPT, mean ± SEM n = 3). Electrophysiological recordings demonstrated that the cells exhibited mature functional properties with trains of tetrodotoxin (TTX)-sensitive action potentials and whole cell Na^+ and K^+ currents (Figure 1E; Figures S1A–S1D available online, n = 9/9). After further maturation, the neurons received synaptic input and exhibited spontaneous postsynaptic currents, which were blocked by the glutamate receptor antagonists NBQX and D-AP5, but not by the $GABA_A$ receptor antagonist picrotoxin (Figure 1F, n = 8/8, day 35). We could not detect any spontaneous inhibitory PSCs in the neurons (n = 0/12).

To determine the regional identity of the neural progenitors obtained using this protocol, we directly compared gene expression in different areas of the developing human brain to the neural progenitors obtained from the hESCs. First, we established a quantitative RT-PCR (qRT-PCR) primer panel for more than 30 genes previously reported to be expressed in distinct regions of the developing mouse brain using a collection of subdissected human fetal neural tube tissue samples from week 7.5–8 postconception (pc) (Table S1), and confirmed that these genes showed a similar regionalized expression pattern in the developing human neural tube (Figures 1G and S1E). Using our primer panel as a readout for regional identity, we established that the hESC-derived neural progenitors showed a gene expression profile consistent with a telencephalic identity, expressing genes such as *OTX2*, *FOXG1*, *SIX3*, *NKX2.1*, and *GSX2* in the absence of markers specific for midbrain and hindbrain (Figure 1G). In accordance with the anterior neuroectodermal gene expression profile of our cultures and the fact that the rostral part of the neural tube is void of a floor plate structure (Placzek and Briscoe, 2005), we did not observe induction of floor plate markers when ventralizing our cultures with a high potency form of SHH (Figure 1G). We hypothesized that caudalizing agents were necessary to generate floor plate cells from more posterior brain regions.

Dose-Dependent Activation of Canonical WNT Signaling Is Sufficient to Mimic Positional Patterning of the Neural Tube in Differentiating hESCs

Members of the WNT family are involved in early caudalization of the cells in the neural plate (Nordström et al., 2002). The canonical WNT signaling pathway depends on inhibition of GSK3 for stabilization and activation of β-catenin. Accordingly, chemical inhibition of GSK3 can activate canonical WNT signaling and induce expression of downstream WNT targets (Frame and Cohen, 2001). We tested the GSK3 inhibitor CT99021 (CT), and confirmed that it activated canonical WNT signaling in differentiating hESC in a dose-dependent manner, as shown by increased nuclear accumulation of β-catenin and activation of the WNT target gene *LEF1* (Figures 2A and 2B). We also ensured that neural induction and maturation was unaffected by the compound by monitoring expression of the neuronal markers *MAP2* and *SYP* throughout the dose-response curve (Figures S2B and S2C).

We next examined the gene expression profile of neural progenitors formed at different concentrations of the GSK3 inhibitor. When compared to expression profiles of the subdissected human neural tube, we found that we could obtain neural progenitors from all regions of the rostrocaudal axis ranging from telencephalon (CT = 0 μM) to posterior hindbrain (CT = 4 μM, Figures 2C and S2A). At CT concentrations below 0.4 μM, the cultures expressed high levels of telencephalic markers *FOXG1*, *LHX2*, *DLX2*, *NKX2.1*, *GSX2*, and *SIX3* in the absence of any markers specific for midbrain and hindbrain. The gene *IRX3*, which is expressed caudal to the zona limitans interthalamica, only appeared at concentrations above 0.4 μM. *OTX2*, which is expressed rostral to the midbrain-hindbrain boundary, was highly expressed at CT concentrations below 1 μM and decreased to undetectable levels above this concentration. The dramatic drop in *OTX2* expression coincided with a peak in *WNT1* expression, which is expressed at the midbrain-hindbrain boundary. These markers indicated that CT concentrations below 1 μM led to rostral identities, whereas CT concentrations above 1 μM led to the production of cell fates caudal to the midbrain-hindbrain boundary. Indeed, hindbrain markers *GBX2*, *HOXA2*, and *HOXA4* were only expressed at CT concentrations of 1–4 μM. In line with the expression pattern of rostral and caudal markers, we observed induction of midbrain fates at a very narrow concentration range of 0.7–0.8 μM. This was evident as peaks of expression of *PAX5*, *LHX1*, *LMX1A*, *LMX1B*, *SIM1*, *EN1*, and *EN2* (Figures 2C and S2A). We established that most genes were expressed at similar levels in our regionalized cultures as in equivalent regions of the human fetal brain (PC week 7.5–8) (Figure S1). When the cells were differentiated toward diencephalic, midbrain, and hindbrain fates (CT 0.4–2 μM), we observed a significant induction of floor plate markers *FOXA2*, *FOXA1*, *SHH*, and *CORIN*, congruent with an existing floor plate structure in these regions (Figures 2C and S2A). To confirm the robustness of our protocol, we repeated the differentiations in another hESC line, SA121 (Heins et al., 2006), and obtained an identical rostrocaudal differentiation pattern (Figure S2D).

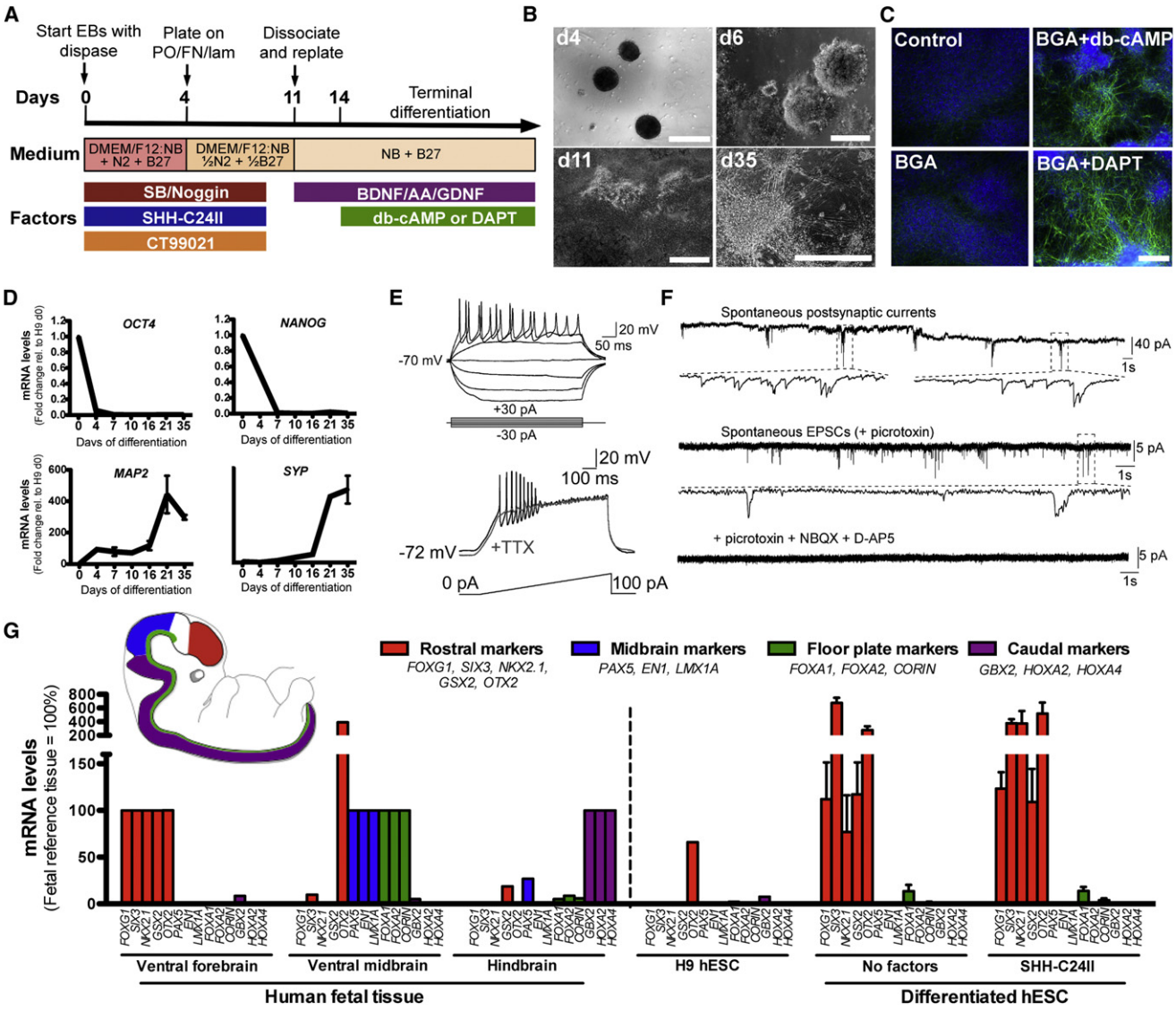

Figure 1. Protocol for Neural Differentiation of hESCs

(A) Overview of differentiation protocol for hESCs. NB, neurobasal; AA, ascorbic acid.

(B) Bright-field images of differentiated cells at different days of differentiation.

(C) Only differentiation in the presence of db-cAMP or DAPT from day 14–30 yielded cultures rich in MAP2 (green). BGA = BDNF+GDNF+AA.

(D) Graphs show mRNA levels of pluripotency markers *OCT4* and *NANOG* and neuronal markers *MAP2* and *SYP* during differentiation, relative to undifferentiated H9 hESCs (= d0).

(E) Representative traces of membrane potential changes recorded in current-clamp mode showing trains of action potentials (upper panel), and TTX-inhibited trains of action potentials generated in response to a depolarizing current-ramp (lower panel). Action potentials were detected in 9 out of 9 recorded neurons (d25).

(F) Representative traces of spontaneous postsynaptic currents (PSCs) recorded at a holding potential of −70 mV in the presence or absence of the $GABA_A$ receptor antagonist picrotoxin or the glutamate receptor antagonists, NBQX and D-AP5 (n = 8, d35).

(G) Gene expression in human fetal brain and H9 cultures differentiated in the absence or presence of 200 ng/ml SHH. All expression levels are normalized to levels detected in human tissue (= 100%). Red: Rostral markers (normalized to forebrain), blue and green: midbrain markers and floor plate markers, respectively (normalized to midbrain), and purple: caudal markers (normalized to hindbrain). Data are represented as mean ± SEM, n = 3 for differentiated hESCs. For tissue, n = 1. See also Figure S1 and Table S1.

Control of Rostrocaudal Fates Can Be Combined with Control of Dorsoventral Fates

To explore if it was possible to also control the dorsoventral range of cell fates at any given rostrocaudal position, we administered varying concentrations of SHH (0, 200, or 500 ng/ml) combined with a fixed concentration of CT (0.7 μM = midbrain fate). Since noggin and SB431542 are potent inhibitors of bone morphogenetic protein (BMP) signaling, we included a SHH-free condition in which noggin and SB431542 (NSB) were withdrawn from the cells after 4 days of differentiation to allow for activation of

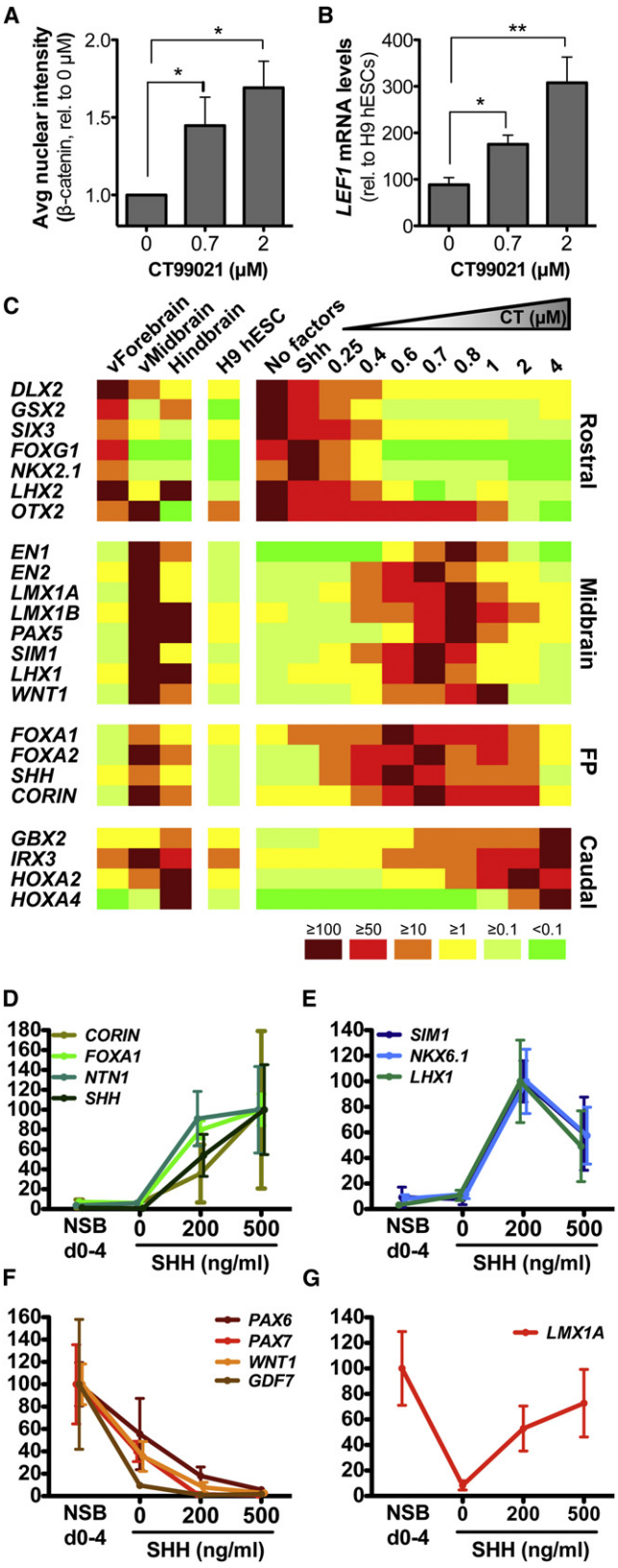

BMP signaling in the cultures. We observed that floor plate markers *FOXA1*, *NTN1*, *CORIN*, and *SHH* as well as basal plate markers *SIM1*, *NKX6.1*, and *LHX1* were only expressed in the presence of SHH (Figures 2D and 2E). While there was a trend for expression of floor plate markers to increase with increasing concentrations of SHH (Figure 2D), the basal plate markers showed a tendency to decrease (Figure 2E). In the absence of SHH, *PAX6* as well as roof plate markers *GDF7*, *PAX7*, and *WNT1* were expressed (Figure 2F). Induction of roof plate markers was particularly pronounced when NSB was withdrawn from the medium on day 4 of differentiation (NSB d0–4). The transcription factor *LMX1A* was induced by SHH and also by NSB withdrawal, reflecting the endogenous expression of LMX1A, which is present in both the roof plate and floor plate of the developing human midbrain (Figure 2G). Pan-midbrain markers and hindbrain markers *OTX2* and *GBX2* were not significantly affected by patterning across the dorsoventral axis (Figure S2E).

Transplanted Neural Progenitors of Rostral, Midbrain, and Caudal Fates Survive and Form Neuron-Rich, Tumor-free Grafts in the Adult Rat Brain

We next transplanted neural progenitors of distinct positional identity after 10 or 16 days of differentiation into the striatum of adult rats. Groups of rats were transplanted with differentiated hESCs corresponding to three different ventralized regional fates: rostral d10 (SHH, n = 4), midbrain = VM d10 and d16 (SHH + 0.7 μM CT, n = 16 and n = 16, respectively), and caudal d10 (SHH + 2 μM CT, n = 7). Six weeks posttransplantation, we observed that all of the grafted animals (total of 43) had surviving transplants and none of the grafts showed signs of aberrant features such as tumor formation or necrosis, indicating that the transplanted cells were well tolerated and contained no obvious contamination of undifferentiated hESCs. The VM-specified cells tended to form the largest transplants and grafting of VM-specified cells on day 16 of differentiation did not affect the graft size or survival compared to day 10 (Figures 3A–3C, 3G, and 3H). After 6 weeks, the grafts from all fates were rich in NESTIN expression, indicating the presence of neural progenitors (Figure 3I), which was also supported by the presence of some proliferating cells at this time point. The forebrain group

Figure 2. Regionalization of H9 Cultures with CT99021

(A and B) H9 cells differentiated for 24 hr in the presence of CT showed (A) increased nuclear intensity of β-catenin immunoreactivity (n = 4), see also Figure S5, and (B) upregulated mRNA levels of the WNT signaling target *LEF1* (n = 4). *p < 0.05, **p < 0.01, Student's t test.

(C) Gene expression of H9 cells differentiated in the absence of factors, or in the presence of SHH combined with CT (from 0 to 4 μM). For each gene, the expression levels were normalized to the cell sample with the highest level observed (= 100), and the values have been color-coded as shown. Comparative expression in human fetal brain samples and in undifferentiated hESCs is shown on the left side of the heatmap (v = ventral). n = 4–5.

(D–G) Dorsoventral gene expression with varying SHH and BMP levels for (D) floor plate markers, (E) basal plate markers, (F) dorsal markers, and (G) the transcription factor LMX1A, which is expressed in both the roof plate and floor plate region. All expression values are represented as mean fold change ± SEM relative to the differentiated sample with the highest expression level (= 100), n = 3–4. See also Figure S2 for full graphs of rostrocaudal patterning and Table S1 for primer sequences.

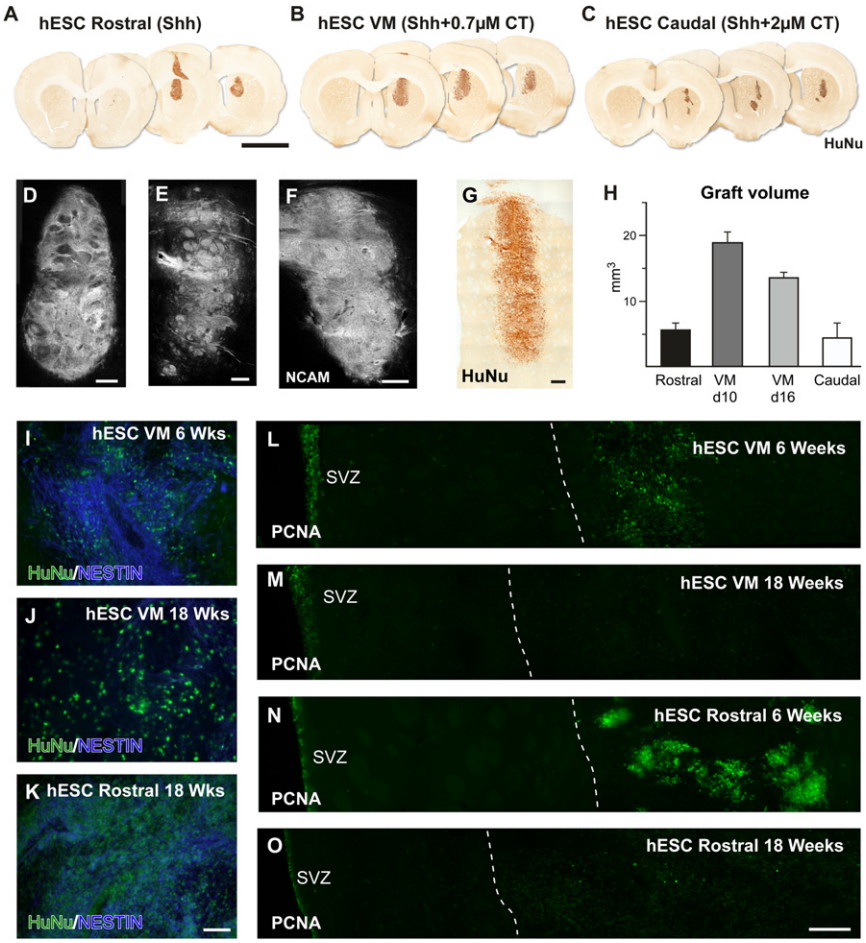

Figure 3. Overview of Survival and Proliferation in Grafts from Regionally Specified hESCs at 6 and 18 Weeks Posttransplantation

(A–C) Grafts resulting from hESCs differentiated for 10 days in vitro patterned toward rostral (SHH), VM (SHH + 0.7 μM CT), or caudal fates (SHH + 2 μM CT).

(D–F) All regions generated neuron-rich grafts as visualized with human-specific NCAM.

(G) hESCs differentiated for 16 days in vitro generated similar grafts.

(H) Assessment of graft volume showed slightly larger grafts in the VM-patterned groups.

(I and J) Neural maturation was assessed at 6 (I) and 18 (J) weeks in the VM condition, with a decrease in expression of NESTIN$^+$ cells at the later time point. Data are presented as mean ± SEM.

(K) In the rostral fate, immature neural progenitors were present also 18 weeks posttransplantation.

(L–O) Ongoing proliferation was assessed using PCNA, with the host subventricular zone (SVZ) used as an internal control (graft-host border delineated with a dashed line). At 6 weeks, both VM and rostral conditions showed ongoing proliferation, but after 18 weeks only rare proliferating cells could be detected in VM group.

Scale: Coronal overlays in (A)–(C) = 4 mm; (D)–(G) = 250 μm; (I)–(K) = 75 μm; (L)–(O) = 150 μm. See also Figure S3 for subtype analyses and graft densities.

contained proliferating PCNA$^+$ cells in characteristic rosette-like structures, whereas PCNA$^+$ cells in the midbrain and caudal grafts were dispersed throughout the graft (Figures 3L, 3N, and S3). All grafts contained a high proportion of neurons as determined by staining for human-specific neural cell adhesion molecule (hNCAM) (Figures 3D–3F). The majority of the neuronal innervation was restricted to the graft core in all three groups although we also observed an affinity for axonal outgrowth in white matter tracts, such as the corpus callosum. At 6 weeks, hNCAM$^+$ fibers could be detected in the internal capsule. Additionally, the forebrain transplants showed some fibers entering the thalamus, whereas the midbrain group more extensively innervated the striatum and some projections were detected in the amygdala and SNr (Figure S4), similar to what has been observed in xenografts of forebrain and midbrain tissue, respectively (Isacson et al., 1995; Wictorin et al., 1990, 1992).

A High Purity of Transplantable mesDA Progenitors Are Formed at a Narrow Concentration Range of GSK3 Inhibitor

To investigate if the regionalizing progenitors could give rise to authentic and functional neurons, we focused the study on the production of mesencephalic DA (mesDA) neurons. In the developing embryo, the mesDA progenitors arise from the floor plate and coexpress FOXA2 and LMX1A (Andersson et al., 2006; Ferri et al., 2007; Hebsgaard et al., 2009; Nelander et al., 2009; Bonilla et al., 2008; Ono et al., 2007). As determined from our gene expression analysis, midbrain floor plate markers were efficiently induced at a narrow concentration range of 0.7–0.8 μM CT in combination with SHH (Figures 2C and S2A). Immunocytochemical analysis confirmed that FOXA2 and LMX1A protein were abundantly coexpressed in the VM condition, but not in the more rostral or caudal hESC-derived progenitors in vitro (Figure 4A). The FOXA2$^+$/LMX1A$^+$ cells in our cultures also expressed the midbrain marker EN1 (Figure 4B) and, like their in vivo counterparts, coexpressed CORIN, thus confirming their floor plate identity (Figures 4E and 4F). The regionalized phenotype of the progenitors was maintained after grafting as the majority of cells in the midbrain group coexpressed LMX1A and FOXA2 at 6 weeks after grafting, whereas none could be detected in the forebrain or hindbrain groups (Figure 4C). In line with this, VM-specified progenitors generated high numbers of DA neurons both in vitro and in vivo, whereas TH$^+$ neurons were absent in equivalent grafts from forebrain- and hindbrain-specified progenitors (Figures 4G and S3).

To confirm the authenticity of our stem cell-derived VM progenitors, we performed a direct histological comparison of hESC-derived VM and human fetal VM at 6 weeks after grafting into the 6-hydroxydopamine (6-OHDA)-lesioned rat striatum. The fetal VM was subdissected from human embryos age

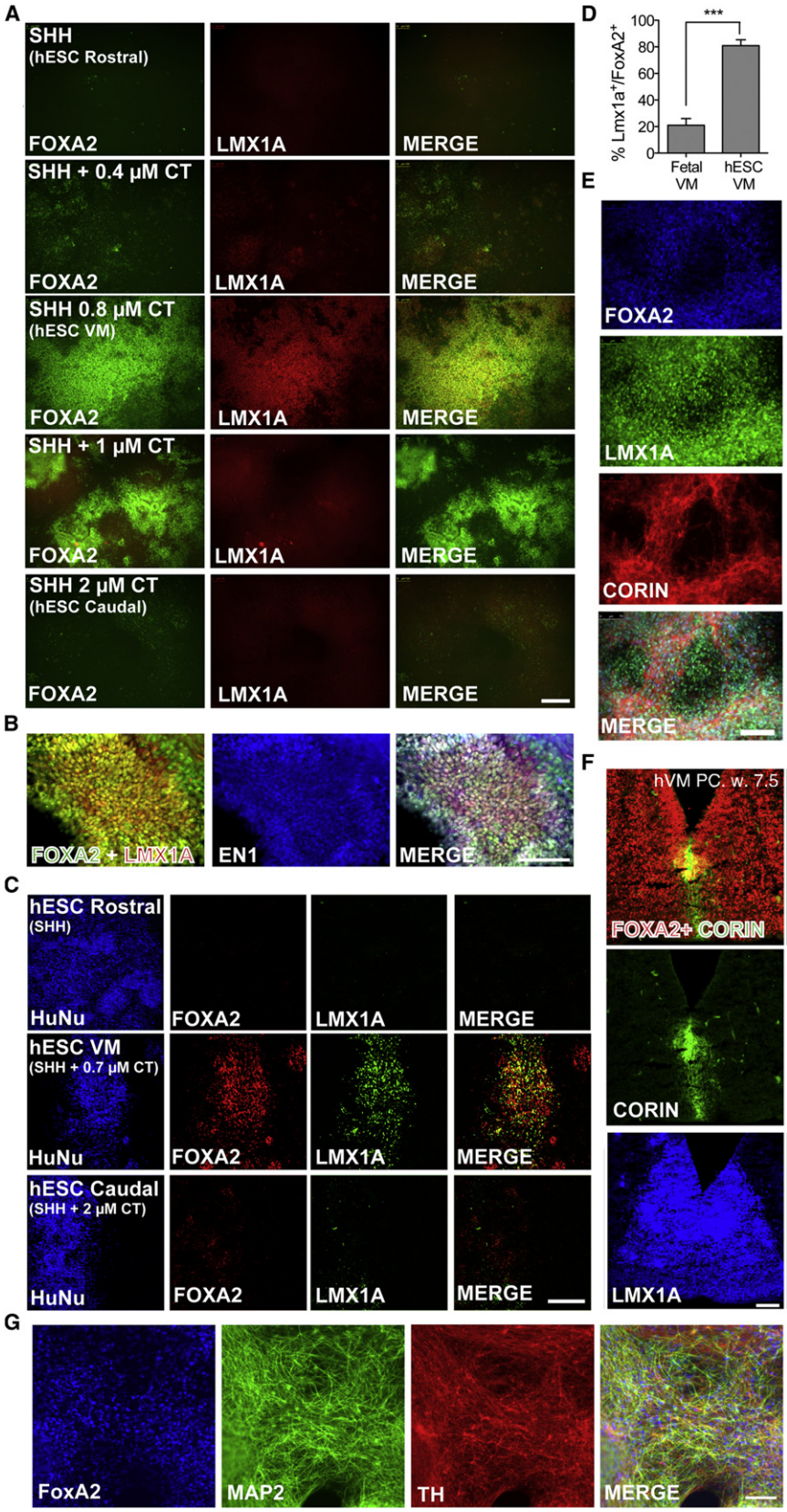

Figure 4. Specification of VM Cells in Differentiated hESCs

(A) Cells expressing FOXA2 and LMX1A were abundant only when hESCs were differentiated in the presence of SHH and 0.7–0.8 μM CT (d11 of differentiation).

(B) These cells also expressed the midbrain marker EN1.

(C) VM-patterned cells maintained expression of FOXA2 and LMX1A 6 weeks after grafting into rat brain.

(D) The number of FOXA2/LMX1A double-positive cells was significantly higher in hESC-derived VM cultures compared to dissociated subdissected fetal VM. Data are presented as mean ± SEM. ***$p < 0.001$, Student's t test.

(E) Expression of FOXA2, LMX1A, and CORIN at day 14 in H9 cultures differentiated toward VM fates. The vast majority of cells coexpressed all three markers.

(F) Immunohistochemical analysis of FOXA2, CORIN, and LMX1A in human fetal VM tissue (pc week 7.5). CORIN is localized to mesDA progenitors in the medial region of the FOXA2/LMX1A domain.

(G) Long-term differentiation of VM-specified cells generated large numbers of $FOXA2^+/TH^+$ neurons (day 42). Scale bar = 200 μm in (A) and (C) and 100 μm in (B) and (E)–(G).

6.5–7 weeks pc, and the transplanted tissue preparation contained an average of 21% of the cells coexpressing LMX1A and FOXA2, compared to 81% for the hESC-derived VM cultures (Figure 4D). Accordingly, the hESCs gave rise to 15-fold more TH^+ neurons in the grafts as compared to fetal VM tissue; 8,338 ± 1,920 (n = 8) versus 558 ± 119 (n = 5) per 100,000 grafted cells ($p < 0.001$) (Figure 6G). A side-by-side comparison of hESC-derived and fetal-derived DA neurons showed virtually indistinguishable phenotypes. EN1 and NURR1 colocalized with LMX1A/FOXA2 and TH/FOXA2 in both the human fetal VM and hESC-derived VM grafts, and many of the neurons from both sources coexpressed TH and aromatic L-amino acid decarboxylase (AADC) (Figures 5A–5F). Close inspection of the morphology of the TH^+ neurons from both cell sources (Figures 5G and 5H) revealed bipolar, angular cell bodies with elongated primary axons located at the periphery of the transplants, which is typical of grafts of fetal VM (Mendez et al., 2005; Thompson et al., 2005). When assessing fiber outgrowth at 6 weeks posttransplantation, we observed similar regional innervation patterns from fetal VM grafts and hESC VM grafts including innervation to the dorsolateral striatum (Figures 5I, 5J, and S4).

Grafts from hESC-Derived VM Progenitors Release DA In Vivo and Reverse Motor Impairments in 6-OHDA-Lesioned Rats

To assess long-term survival and function of the positionally specified hESC-derived progenitors, VM and forebrain patterned cells were grafted in parallel into 6-OHDA-lesioned adult rats and kept under ciclosporin-mediated immunosuppression for the duration of the experiment. After 18 weeks, the forebrain cells remained tightly clustered in the graft, whereas the VM-patterned cells had dispersed into the host striatum; the density of VM-patterned grafts were 1165 $HuNu^{+-}$ nuclei/mm^2 at 6 weeks compared to 634 $HuNu^+$ nuclei/mm^2 at 18 weeks (n = 4 per group, see also Figure S3). At this point, the midbrain group contained only a few NESTIN-expressing cells and cell proliferation was minimal (Figures 3J and 3M). Pockets of proliferating cells were still present in the forebrain group, which also contained some NESTIN-expressing progenitors, indicating a prolonged proliferation and slower maturation of the forebrain-specified grafts (Figures 3K and 3O). The rostral grafts remained devoid of DA neurons after 18 weeks, whereas 54.2% ± 2.5% of cells in the hESC VM grafts were TH positive (% $TH^+/HuNu^+$, mean ± SEM, n = 3, see also Figures 6A and 6B). Both the total number of DA neurons (Figure 6G) and the graft-derived innervation of the host striatum increased markedly between 6 and 18 weeks posttransplantation in grafts of VM-patterned hESCs (Figures 6D and 6D′ compared to Figure 5J). The neurons displayed a morphology characteristic of mesDA neurons and a large proportion also expressed GIRK2, typical of nigral A9 DA neurons (Thompson et al., 2005) (Figure 6F). In vivo amperometric measurements showed that the grafts derived from the VM group, but not the forebrain group, released dopamine 18 weeks after transplantation (Figure 6C) at levels comparable to previous reports of grafts of human fetal VM and mouse ES cells (Rodríguez-Gómez et al., 2007; Strömberg et al., 1989). Accordingly, hESC-derived VM patterned cells reversed amphetamine-induced rotational asymmetry in 6-OHDA-lesioned rats, while the rats grafted with forebrain patterned cells showed no change in rotational response after 12 or 16 weeks (Group × Time, $\chi^2_{(10,96)} = 75.09$, $p < 0.0001$; posttransplantation difference confirmed using a Bonferroni-adjusted one-way ANOVA with a Tukey post hoc test, $p < 0.01$) (Figure 6H). In the cylinder test, a measure of forelimb akinesia, the rats grafted with VM-patterned cells showed a significant increase in touches using the affected paw when compared to the lesion control group, while the forebrain patterned cells did not (Group, $F_{(2,14)} = 5.00$, $p < 0.05$; confirmed using a Tukey post hoc test) (Figure 6I).

DISCUSSION

In this study, we combined dual SMAD inhibition with EB formation (Chambers et al., 2009; Nat et al., 2007) to achieve a rapid and efficient neural differentiation protocol devoid of any manual picking steps and undefined biological components. In the absence of positional cues, the progenitors defaulted into an anterior neural identity similar to what has been reported for other ES differentiation paradigms (Gaspard et al., 2008; Li et al., 2009; Pankratz et al., 2007). Concurrent chemical activation of the canonical WNT pathway caused a progressive dose-dependent induction of caudal cell fates analogous to the caudalizing effect of WNTs in the early developing neural tube (Nordström et al., 2002). Although WNT signaling is also known to be involved in dorsoventral patterning (Ulloa and Martí, 2010), we could nonetheless accurately control the full range of fates from floor plate to roof plate when combining WNT activation with modulation of SHH and BMP signaling. Therefore, our system can be used to rapidly generate region-specific neural progenitors with a high similarity to neural progenitors from different levels of the developing human neural tube, and with the capacity to mature into subtype-specific neurons.

A particularly striking observation was that our neural progenitors could be grafted into the rodent brain as early as 10 days after neural induction with good survival, high neuronal differentiation, and maintained regional specification. Despite the short culture time prior to transplantation, the grafts showed no signs of tumor formation or necrosis, which are features otherwise commonly associated with transplantation of progenitors derived from pluripotent stem cells (Miura et al., 2009; Roy et al., 2006). This is a significant advancement over existing protocols (Aubry et al., 2008; Brederlau et al., 2006; Chiba et al., 2008; Kriks et al., 2011; Seminatore et al., 2010) since it eliminates the need for prolonged culturing prior to transplantation, making it cost effective, and reducing the variation and asynchrony associated with extended in vitro differentiation prior to transplantation.

By selecting the appropriate combination of developmentally relevant extrinsic patterning agents, we could generate hESC-derived neural progenitors with the same gene and protein expression profile as DA progenitors in the developing human VM. In our protocol, 0.7–0.8 μM CT represented the optimal concentration for inducing midbrain fates and higher concentrations yielded progenitors of a more caudal identity, as determined by onset of expression of *GBX2* and other caudal

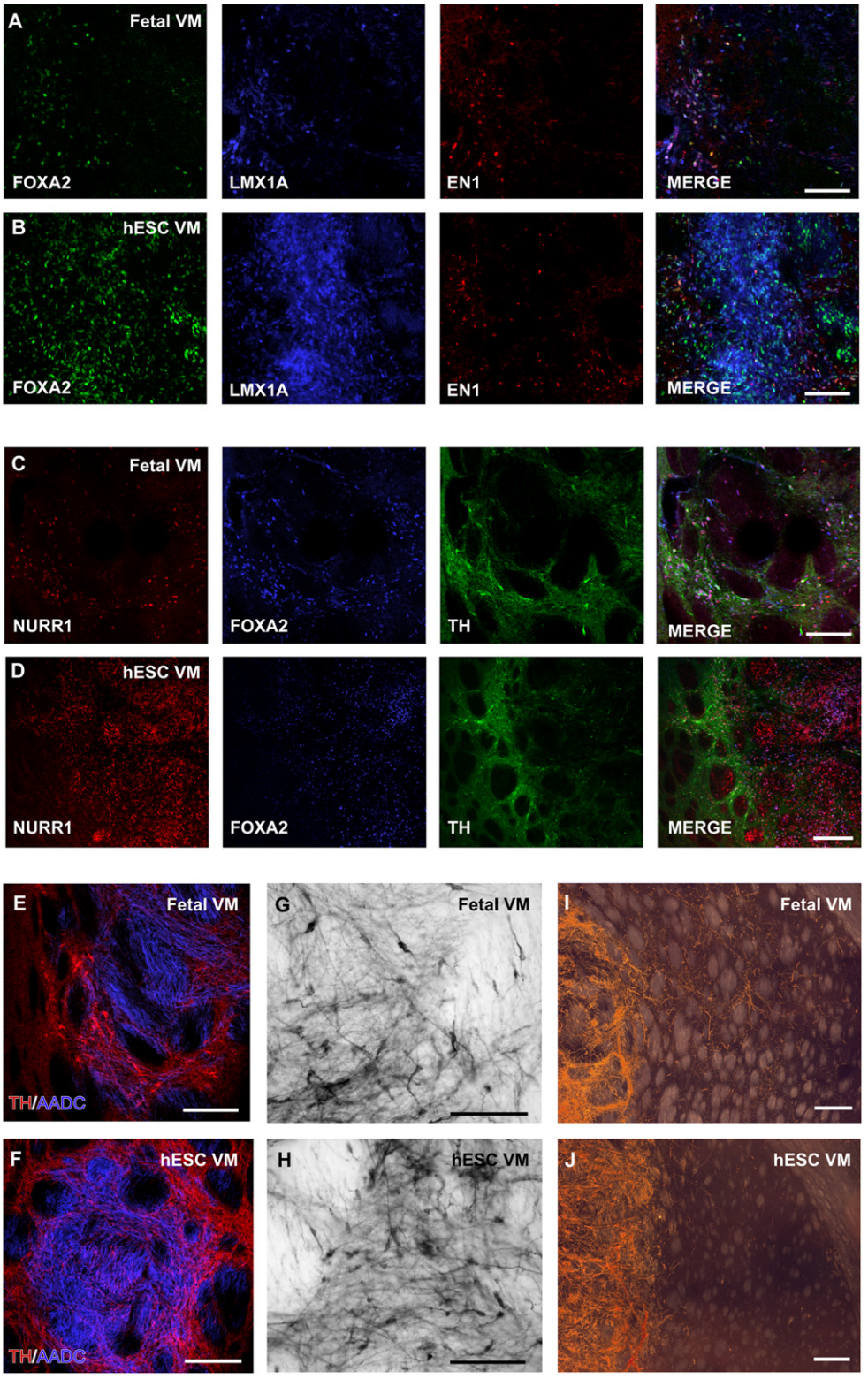

Figure 5. Phenotypic Comparison of Human Fetal VM Grafts and Their hESC-Derived Counterparts

(A–D) The phenotypic profile of transplants from (A) fetal VM and (B) hESC-derived VM cells were compared using a selection of regional markers identifying mesDA neurons: EN1, LMX1A and FOXA2. Mature markers TH, NURR1 and FOXA2 were also compared between (C) the fetal VM and (D) their hESC-derived counterparts.

markers. This finding differs from a recent study in which mesDA neurons were obtained via dual SMAD inhibition using 3 μM of the same CT compound (Kriks et al., 2011). We speculate that this discrepancy may be due to the fact that CT was present from day 0 of differentiation in our protocol, whereas treatment was initiated 2 days later in the study of Kriks et al. The presence of undefined components in the KSR and matrigel used in the latter study might also contribute to differential modulation of external patterning effects.

From the side-by-side comparisons of hESCs and fetal VM cells, we found that our hESC-derived progenitors had virtually indistinguishable gene and protein expression. Likewise, 6 weeks after transplantation, the neurons obtained from the two cell sources had a similar morphology, expressed the same mature DA markers and mesDA-specific proteins, and projected to the same target structures. After 18 weeks of maturation of the midbrain-patterned hESC-derived grafts, the cells had dispersed into the host parenchyma, where they extensively innervated the striatum and released DA. Their functional efficacy was confirmed through complete reversal of amphetamine-induced rotational asymmetry, as well as increased use of the affected forelimb in a unilateral animal model of PD, matching what has previously been established using human fetal VM (Brundin et al., 1988).

With few exceptions (Cooper et al., 2010; Kriks et al., 2011), most previously published protocols derive DA neurons from cultures mainly comprised of PAX6 expressing neural progenitors (Koch et al., 2009b; Perrier et al., 2004; Roy et al., 2006; Sonntag et al., 2007; Swistowski et al., 2009). PAX6-derived DA neurons have since been shown to be mainly of a diencephalic DA subtype (Cooper et al., 2010), but for cell therapy in PD the A9 mesDA phenotype is essential (Grealish et al., 2010; Zuddas et al., 1991). The improvement in motor function of the mesDA neurons generated using our protocol is comparable to what was reported by Kriks et al. (2011) when assayed in a rat model of PD. These studies suggest that protocols, which recapitulate developmental pathways, are necessary to generate authentic and functional DA neurons. From a clinical perspective, advantages with our protocol are that we have extensively established the authenticity of progenitors and neurons using fetal VM as comparison, confirmed DA release, avoided the use of undefined components in the media, and that the cells required a much shorter culturing time in vitro prior to grafting.

In summary, we show that dose-dependent activation of WNT signaling in hESCs is a simple and efficient method for generating transplantable and authentic progenitors from the entire rostrocaudal neural axis. The hESC-derived progenitors and resulting neurons obtained via our protocol closely resembled their fetal counterparts, making them useful as a model system for studies of human fetal brain development and also for developing successful stem cell-based therapies for neurodegenerative diseases.

EXPERIMENTAL PROCEDURES

Human Fetal Tissue

Human fetal tissue was obtained from subdissections of aborted fetuses (pc week 6–8, determined by crown-rump length) donated under informed consent with approval of Lund Regional Ethical Committee and the Swedish national board of health and welfare. Immunohistochemistry was performed as previously described (Nelander et al., 2009). For quantification of LMX1A and FOXA2, human fetal VM was subdissected and triturated to yield single-cell suspensions. The cells were immobilized on glass slides by cytospin followed by fixation in 4% paraformaldehyde (PFA) for immunocytochemistry. Before transplantation, the human fetal VM was stored in hibernation medium at 4°C overnight followed by dissociation at 37°C for 10–15 min in 0.1% trypsin/0.05% DNase diluted in HBSS (Invitrogen). The cells were washed three times before transplantation.

Cell Culture and Differentiation Procedure

All cell culture reagents were from Invitrogen unless stated otherwise. Human ESCs H9 (WA09, passage 31–45 (Thomson et al., 1998) and SA121, passage 25–35 (Heins et al., 2006) were maintained on γ-irradiated mouse embryonic fibroblasts in DMEM/F12, 20% KSR, 0.05 mM 2-mercaptoethanol, 0.5% Pen/Strep and 10 ng/ml FGF-2 (R&D Systems). The cells were passaged once weekly with dispase (5 mg/ml, Stemcell Tech.). For differentiation, the colonies were detached with dispase and EBs were formed in DMEM/F12:Neurobasal (1:1), N2 supplement (1:100), and B27 supplement without vitamin A (1:50). Rock inhibitor (Y-27632, 10 μM, Tocris Biochem.) was present from d0 to d2. On d4 of differentiation, the EBs were plated in DMEM/F12:Neurobasal (1:1), N2 supplement (1:200), and B27 supplement without vitamin A (1:100) onto plasticware coated with polyornithine (PO), fibronectin (FN), and laminin (lam). From d0 to d9, SB431542 (10 μM, Tocris Biochem.) and Noggin (200 ng/ml, R&D) was present in the medium for neuralization (unless stated otherwise in the text). Patterning factors SHH-C24II (R&D, 200 ng/ml unless stated otherwise), and CT99021 (Axon Medchem) were also present in the medium from d0 to d9. On d11 of differentiation, the cell clusters were dissociated to single cells with accutase and replated onto dry PO/FN/lam-coated plates in droplets of 5–15,000 cells/μl in Neurobasal, B27 supplement without vitamin A (1:50), brain-derived neurotrophic factor (BDNF) (20 ng/ml), glial cell line-derived neurotrophic factor (GDNF) (10 ng/ml), and ascorbic acid (200 μM). From d14 and onward, db-cAMP (0.5 mM) or DAPT (2.5 μM) was added to the medium for terminal differentiation.

Quantitative RT-PCR

Quantitative RT-PCR was performed using Sybr Green detection with the LightCycler 480 instrument (Roche). See Extended Experimental Procedures for primer sequences and details.

Electrophysiology

Plated cells were constantly perfused with heated (32°C–34°C), gassed (95% O_2, 5% CO_2) solution (pH 7.2–7.4, 295–300 mOsm) containing (in mM): 119 NaCl, 2.5 KCl, 1.3 $MgSO_4$, 2.5 $CaCl_2$, 26 $NaHCO_3$, 1.25 NaH_2PO_4, and 25 glucose. Cells for recording were visualized under infrared light with differential interference contrast using an Olympus upright microscope equipped with a digital camera and a 40× water-immersion lens. Recording pipettes were filled with solution (pH 7.2–7.4, 295–300 mOsm) containing (in mM): 122.5 potassium gluconate, 12.5 KCl, 10.0 KOH-HEPES, 0.2 KOH-EGTA, 2 MgATP, 0.3 Na3-GTP, and 8 NaCl, resulting in pipette resistances of 3–5 MΩ. For measurements of spontaneous inhibitory postsynaptic currents recording pipettes contained (in mM): 135.0 CsCl, 10.0 CsOH, 0.2 CsOH-EGTA, 2 Mg-ATP, 0.3 Na3-GTP, 8 NaCl, and 5 lidocaine Nethyl bromide (QX-314, Tocris), resulting in pipette resistances of 3–4 MΩ. Postsynaptic currents were measured in voltage clamp at −70 mV. GABAA receptors were blocked using 100 μM picrotoxin (PTX, Tocris). N-Methyl-D-aspartate and α-amino-3-hydroxy-5-methyl-4-isoxazolepropionic acid (AMPA) receptors were blocked using 50 μM

(E and F) Markers of dopamine metabolism were assessed by expression of TH and AADC.
(G and H) Typical mesDA morphology was distinguished using TH immunohistochemistry.
(I and J) Dark-field images show innervation of the host striatum.
Scale bar = 200 μm. See also Figure S4 for innervation patterns.

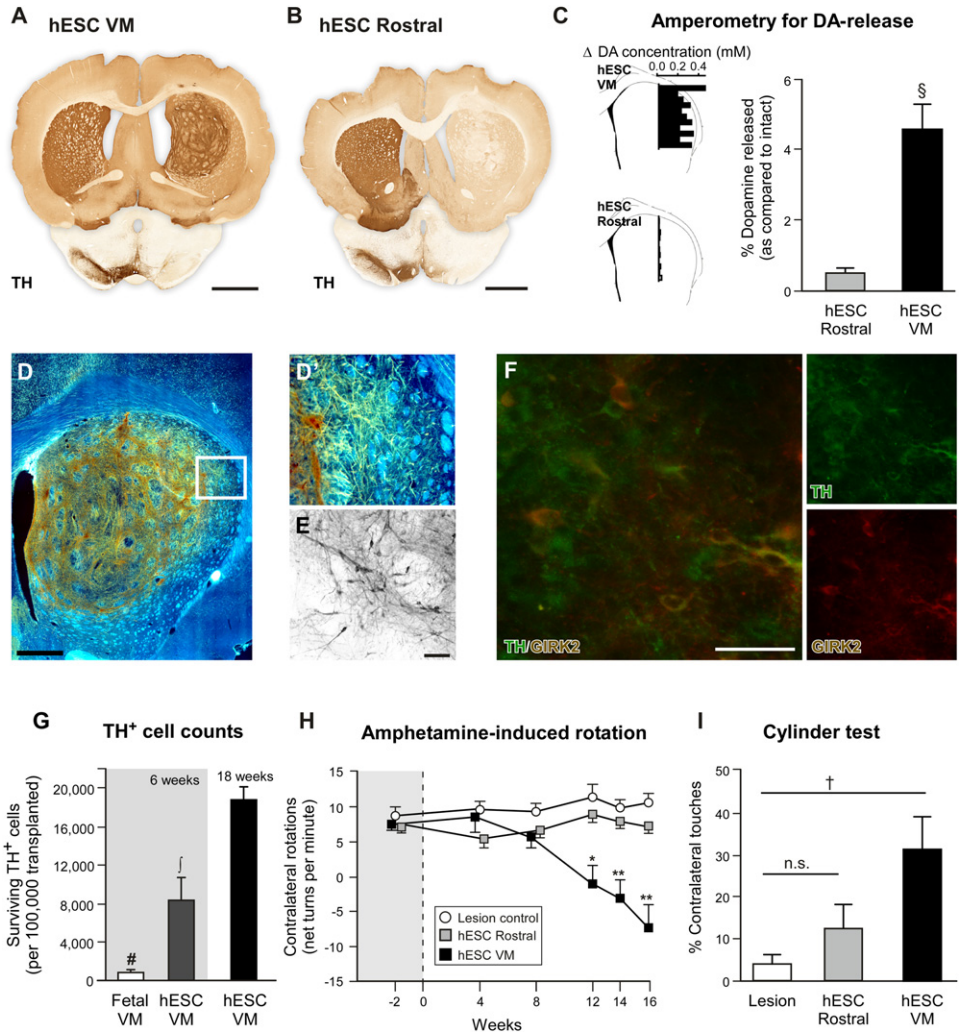

Figure 6. hESC-Derived VM Grafts Release Dopamine and Reverse Motor Deficits at 18 Weeks Posttransplantation in a Rat Model of Parkinson's Disease

(A and B) Adult rats were subjected to 6-OHDA lesions for unilateral depletion of TH^+ neurons, and subsequently received transplants of hESC-derived cells patterned toward (A) VM or (B) rostral fates. Coronal sections from 18 weeks posttransplantation show that VM cells efficiently differentiated into DAergic neurons, whereas the rostral cells did not.

(C) Dopamine release was measured using in vivo amperometry at a series of dorsoventral depths within the grafted striatum (as depicted). Potassium-evoked release events were only observed in the hESC VM group. Recordings from individual animals that exemplify each group are shown to the left and DA release from all recorded animals (n = 3 from each group) to the right.

(D) Dark-field overview of TH^+ graft-derived innervation from an animal transplanted with hESC VM cells showed extensive innervation of the host striatum after 18 weeks survival, in particular, the dorsolateral striatum (D′).

(E) TH immunohistochemistry revealed angular neurons at the graft edge, extending processes into the host striatum.

(F) $GIRK2^+/TH^+$ neurons were frequently observed in grafts of hESC VM cells.

(G) Estimation of surviving TH^+ neurons normalized to number of cells grafted, n = 4 for all groups.

(H) Animals transplanted with hESC VM cells (n = 6) normalized amphetamine-induced rotation after 12 weeks posttransplantation while rats with grafts of rostral cells (n = 7) showed no reduction in drug-induced rotations at any time point analyzed (n = 6 for lesion control).

(I) hESC VM grafted animals (n = 6) displayed significantly more paw touches than lesion control rats (n = 6) when tested in the cylinder at 14 weeks posttransplantation, while the animals receiving hESC rostral grafts (n = 7) showed no significant difference from controls.

All data in graphs are presented as mean ± SEM. *$p < 0.001$ (hESC VM versus hESC rostral and lesion control), **$p < 0.0001$ (hESC VM versus hESC rostral and lesion control), †$p < 0.05$ (hESC VM versus lesion control), §$p < 0.0001$ (hESC VM versus hESC rostral), #$p < 0.0001$ (Fetal VM versus hESC VM 6 and 18 weeks), ∫$p < 0.0001$ (hESC VM 6 versus hESC VM 18 weeks).

(2R)-amino-5-phosphonovaleric acid (D-AP5, Tocris) and 5 μM 2,3-dihydroxy-6-nitro-7-sulfamoylbenzo[f]quinoxaline-2,3-dione (NBQX, Tocris), respectively. Voltage-gated sodium and potassium channels were blocked with 1 μM tetrodotoxin (TTX, Tocris) and 2 mM tetraethylammonium (TEA, Sigma), respectively.

Lesions and Transplantation Surgery

Adult female Sprague-Dawley rats (225–250 g, Charles River) were housed in a 12-hr-light/dark cycle with ad libitum access to food and water. All experimental procedures were conducted following the guidelines put in place by

the Ethical Committee for the use of Laboratory Animals in Lund University. Surgical procedures were conducted under general anesthesia using a 20:1 fentanyl and medetomidine solution injected intraperitoneally (Apoteksbolaget, Sweden). The rats were made parkinsonian by injecting 6-OHDA into the medial forebrain bundle for complete lesion of the nigrostriatal dopaminergic pathway in the right hemisphere (see Extended Experimental Procedures). At least 4 weeks postlesion, cells were transplanted into the striatum using a microtransplantation approach as previously described (Nikkhah et al., 2000). For differentiated hESCs, 2 × 1 μl deposits of 75,000 cells/μl (total of 150,000 cells) were transplanted for d10, or for d16: 2 × 2 μl deposits of 75,000 cells/μl (total of 300,000 cells). Immunosuppressive treatment was given for the duration of the experiment, in the form of daily intraperitoneal injections of ciclosporin (10 mg/kg), beginning 1 day prior to transplantation.

Immunostaining, Imaging, and Quantifications

For a complete list of antibodies and dilutions used in this study, see Table S2. Nuclear β-catenin intensity in hESCs was quantified through automated image acquisition and analysis using the Cellomics instrument and software from Thermo Scientific (see Figure S5). Each experiment was averaged from two wells with 1,500 analyzed cells in each well. See Extended Experimental Procedures for procedures on quantification of graft volume and number of TH^+ cells in the grafts.

Behavioral Analyses

Amphetamine-induced rotation was performed using automated rotational bowls (AccuScan Instruments). D-Amphetamine sulfate at a dose of 2.5 mg/kg was delivered intraperitoneally and full-body rotations were recorded over a period of 90 min. The data are expressed as net full body turns per minute, where rotation toward the side of the lesion was given a positive value. A two-way ANOVA was performed on amphetamine-induced rotation data using the generalized linear model and the Wald χ^2 test. The cylinder test was performed as a measure of forelimb use, where animals were placed individually in a glass cylinder and spontaneous weight-bearing forepaw contacts with the glass were counted. For in-depth details please refer to Grealish et al. (2010).

Amperometry

Chronoamperometric measurements of evoked dopamine release were performed using Fast Analytical Sensing Technology apparatus (FAST-16, Quanteon LLC, Lexington, KY) coupled to carbon fiber electrodes (SPF1, Quanteon LLC) coated with Nafion (Sigma Aldrich, Sweden) as previously described (Hoffman et al., 1998). Dopamine release was evoked by application of fixed amount (200 nl) 120 mM KCl adjacent to the recording electrode. Dopamine concentration was continuously monitored at 1 Hz. The peak amplitude concentration was calculated using FAST analysis software (Quanteon, LLC). The recording electrode was stereotactically placed at the same anterior-posterior and lateral coordinates as the previous graft implantation surgery. Three KCl ejections (5 min intervals) were made every 250 mm between −3.0 and −5.5 mm from dural surface. The average peak amplitude was calculated from each recording site.

Statistical Analysis

All pooled data are presented as mean ± SEM. Statistical tests and number of biological replicates relevant for individual experiments are stated in Results or in the figures legends.

SUPPLEMENTAL INFORMATION

Supplemental Information includes Extended Experimental Procedures, five figures, and two tables and can be found with this article online at doi:10.1016/j.celrep.2012.04.009.

LICENSING INFORMATION

ACKNOWLEDGMENTS

We thank Ingar Nilsson, Ulla Jarl, Anneli Josefsson, Bengt Mattsson, and Anna-Karin Olden for technical assistance, Z. Kokaia and J. Reimer for collaborative work on the human tissue collection, Prof. Anders Björklund and Dr. Johan Jakobsson for helpful scientific discussions, and Ulrich Pfisterer for experimental help. This study was supported by grants from the European Community's 7th Framework Programme through NeuroStemcell (nr. 22943) and TransEuro (HEALTH-F5-2010-242003), Swedish Research Council; Grant No.: K2011-62X-20390-05-6 (M.P.), StemTherapy (O.L.) 349-2007-8626 (Bagadilico, M.P.) Crafoord Foundation (M.P.), Swedish Parkinson Foundation (M.P.), Kocks Foundation (M.P.), and Segerfalk Foundation (M.P.). A.K. was supported via a postdoctoral grant from the Lundbeck Foundation (R44-A3856).

Received: January 11, 2012
Revised: March 8, 2012
Accepted: April 23, 2012
Published online: May 24, 2012

REFERENCES

Ahrlund-Richter, L., De Luca, M., Marshak, D.R., Munsie, M., Veiga, A., and Rao, M. (2009). Isolation and production of cells suitable for human therapy: challenges ahead. Cell Stem Cell *4*, 20–26.

Andersson, E., Tryggvason, U., Deng, Q., Friling, S., Alekseenko, Z., Robert, B., Perlmann, T., and Ericson, J. (2006). Identification of intrinsic determinants of midbrain dopamine neurons. Cell *124*, 393–405.

Aubry, L., Bugi, A., Lefort, N., Rousseau, F., Peschanski, M., and Perrier, A.L. (2008). Striatal progenitors derived from human ES cells mature into DARPP32 neurons in vitro and in quinolinic acid-lesioned rats. Proc. Natl. Acad. Sci. USA *105*, 16707–16712.

Baker, M. (2011). Stem cells in culture: defining the substrate. Nat. Methods *8*, 293–297.

Bonilla, S., Hall, A.C., Pinto, L., Attardo, A., Götz, M., Huttner, W.B., and Arenas, E. (2008). Identification of midbrain floor plate radial glias-lika cells as dopaminergic progenitors. Glia *56*, 809–820.

Brederlau, A., Correia, A.S., Anisimov, S.V., Elmi, M., Paul, G., Roybon, L., Morizane, A., Bergquist, F., Riebe, I., Nannmark, U., et al. (2006). Transplantation of human embryonic stem cell-derived cells to a rat model of Parkinson's disease: effect of in vitro differentiation on graft survival and teratoma formation. Stem Cells *24*, 1433–1440.

Brundin, P., Strecker, R.E., Widner, H., Clarke, D.J., Nilsson, O.G., Astedt, B., Lindvall, O., and Björklund, A. (1988). Human fetal dopamine neurons grafted in a rat model of Parkinson's disease: immunological aspects, spontaneous and drug-induced behaviour, and dopamine release. Exp. Brain Res. *70*, 192–208.

Chambers, S.M., Fasano, C.A., Papapetrou, E.P., Tomishima, M., Sadelain, M., and Studer, L. (2009). Highly efficient neural conversion of human ES and iPS cells by dual inhibition of SMAD signaling. Nat. Biotechnol. *27*, 275–280.

Chiba, S., Lee, Y.M., Zhou, W., and Freed, C.R. (2008). Noggin enhances dopamine neuron production from human embryonic stem cells and improves behavioral outcome after transplantation into Parkinsonian rats. Stem Cells *26*, 2810–2820.

Cooper, O., Hargus, G., Deleidi, M., Blak, A., Osborn, T., Marlow, E., Lee, K., Levy, A., Perez-Torres, E., Yow, A., and Isacson, O. (2010). Differentiation of human ES and Parkinson's disease iPS cells into ventral midbrain dopaminergic neurons requires a high activity form of SHH, FGF8a and specific regionalization by retinoic acid. Mol. Cell. Neurosci. *45*, 258–266.

Fasano, C.A., Chambers, S.M., Lee, G., Tomishima, M.J., and Studer, L. (2010). Efficient derivation of functional floor plate tissue from human embryonic stem cells. Cell Stem Cell *6*, 336–347.

Ferri, A.L., Lin, W., Mavromatakis, Y.E., Wang, J.C., Sasaki, H., Whitsett, J.A., and Ang, S.L. (2007). Foxa1 and Foxa2 regulate multiple phases of midbrain dopaminergic neuron development in a dosage-dependent manner. Development *134*, 2761–2769.

Frame, S., and Cohen, P. (2001). GSK3 takes centre stage more than 20 years after its discovery. Biochem. J. *359*, 1–16.

Gaspard, N., and Vanderhaeghen, P. (2011). From stem cells to neural networks: recent advances and perspectives for neurodevelopmental disorders. Dev. Med. Child Neurol. *53*, 13–17.

Gaspard, N., Bouschet, T., Hourez, R., Dimidschstein, J., Naeije, G., van den Ameele, J., Espuny-Camacho, I., Herpoel, A., Passante, L., Schiffmann, S.N., et al. (2008). An intrinsic mechanism of corticogenesis from embryonic stem cells. Nature *455*, 351–357.

Grealish, S., Jönsson, M.E., Li, M., Kirik, D., Björklund, A., and Thompson, L.H. (2010). The A9 dopamine neuron component in grafts of ventral mesencephalon is an important determinant for recovery of motor function in a rat model of Parkinson's disease. Brain *133*, 482–495.

Hebsgaard, J.B., Nelander, J., Sabelström, H., Jönsson, M.E., Stott, S., and Parmar, M. (2009). Dopamine neuron precursors within the developing human mesencephalon show radial glial characteristics. Glia *57*, 1648–1658.

Heins, N., Lindahl, A., Karlsson, U., Rehnström, M., Caisander, G., Emanuelsson, K., Hanson, C., Semb, H., Björquist, P., Sartipy, P., and Hyllner, J. (2006). Clonal derivation and characterization of human embryonic stem cell lines. J. Biotechnol. *122*, 511–520.

Hoffman, A.F., Lupica, C.R., and Gerhardt, G.A. (1998). Dopamine transporter activity in the substantia nigra and striatum assessed by high-speed chronoamperometric recordings in brain slices. J. Pharmacol. Exp. Ther. *287*, 487–496.

Isacson, O., Deacon, T.W., Pakzaban, P., Galpern, W.R., Dinsmore, J., and Burns, L.H. (1995). Transplanted xenogeneic neural cells in neurodegenerative disease models exhibit remarkable axonal target specificity and distinct growth patterns of glial and axonal fibres. Nat. Med. *1*, 1189–1194.

Koch, P., Kokaia, Z., Lindvall, O., and Brüstle, O. (2009a). Emerging concepts in neural stem cell research: autologous repair and cell-based disease modelling. Lancet Neurol. *8*, 819–829.

Koch, P., Opitz, T., Steinbeck, J.A., Ladewig, J., and Brüstle, O. (2009b). A rosette-type, self-renewing human ES cell-derived neural stem cell with potential for in vitro instruction and synaptic integration. Proc. Natl. Acad. Sci. USA *106*, 3225–3230.

Kriks, S., Shim, J.W., Piao, J., Ganat, Y.M., Wakeman, D.R., Xie, Z., Carrillo-Reid, L., Auyeung, G., Antonacci, C., Buch, A., et al. (2011). Dopamine neurons derived from human ES cells efficiently engraft in animal models of Parkinson's disease. Nature *480*, 547–551.

Li, X.J., Zhang, X., Johnson, M.A., Wang, Z.B., Lavaute, T., and Zhang, S.C. (2009). Coordination of sonic hedgehog and Wnt signaling determines ventral and dorsal telencephalic neuron types from human embryonic stem cells. Development *136*, 4055–4063.

Mendez, I., Sanchez-Pernaute, R., Cooper, O., Viñuela, A., Ferrari, D., Björklund, L., Dagher, A., and Isacson, O. (2005). Cell type analysis of functional fetal dopamine cell suspension transplants in the striatum and substantia nigra of patients with Parkinson's disease. Brain *128*, 1498–1510.

Miura, K., Okada, Y., Aoi, T., Okada, A., Takahashi, K., Okita, K., Nakagawa, M., Koyanagi, M., Tanabe, K., Ohnuki, M., et al. (2009). Variation in the safety of induced pluripotent stem cell lines. Nat. Biotechnol. *27*, 743–745.

Nat, R., Nilbratt, M., Narkilahti, S., Winblad, B., Hovatta, O., and Nordberg, A. (2007). Neurogenic neuroepithelial and radial glial cells generated from six human embryonic stem cell lines in serum-free suspension and adherent cultures. Glia *55*, 385–399.

Nelander, J., Hebsgaard, J.B., and Parmar, M. (2009). Organization of the human embryonic ventral mesencephalon. Gene Expr. Patterns *9*, 555–561.

Nikkhah, G., Winkler, M., Rödter, A., and Samii, M. (2000). Microtransplantation of nigral dopamine neurons: a "step by step" recipe. In Neuromethods: Cell and Tissue Transplantation in the CNS, S. Dunnett, A. Boulton, and G. Baker, eds. (Totowas, NJ: Humana).

Nordström, U., Jessell, T.M., and Edlund, T. (2002). Progressive induction of caudal neural character by graded Wnt signaling. Nat. Neurosci. *5*, 525–532.

Ono, Y., Nakatani, T., Sakamoto, Y., Mizuhara, E., Minaki, Y., Kumai, M., Hamaguchi, A., Nishimura, M., Inoue, Y., Hayashi, H., et al. (2007). Differences in neurogenic potential in floor plate cells along an anteriorposterior location: midbrain dopaminergic neurons originate from mesencephalic floor plate cells. Development *134*, 3213–3225.

Pankratz, M.T., Li, X.J., Lavaute, T.M., Lyons, E.A., Chen, X., and Zhang, S.C. (2007). Directed neural differentiation of human embryonic stem cells via an obligated primitive anterior stage. Stem Cells *25*, 1511–1520.

Perrier, A.L., Tabar, V., Barberi, T., Rubio, M.E., Bruses, J., Topf, N., Harrison, N.L., and Studer, L. (2004). Derivation of midbrain dopamine neurons from human embryonic stem cells. Proc. Natl. Acad. Sci. USA *101*, 12543–12548.

Placzek, M., and Briscoe, J. (2005). The floor plate: multiple cells, multiple signals. Nat. Rev. Neurosci. *6*, 230–240.

Rodríguez-Gómez, J.A., Lu, J.Q., Velasco, I., Rivera, S., Zoghbi, S.S., Liow, J.S., Musachio, J.L., Chin, F.T., Toyama, H., Seidel, J., et al. (2007). Persistent dopamine functions of neurons derived from embryonic stem cells in a rodent model of Parkinson disease. Stem Cells *25*, 918–928.

Roy, N.S., Cleren, C., Singh, S.K., Yang, L., Beal, M.F., and Goldman, S.A. (2006). Functional engraftment of human ES cell-derived dopaminergic neurons enriched by coculture with telomerase-immortalized midbrain astrocytes. Nat. Med. *12*, 1259–1268.

Seminatore, C., Polentes, J., Ellman, D., Kozubenko, N., Itier, V., Tine, S., Tritschler, L., Brenot, M., Guidou, E., Blondeau, J., et al. (2010). The postischemic environment differentially impacts teratoma or tumor formation after transplantation of human embryonic stem cell-derived neural progenitors. Stroke *41*, 153–159.

Sonntag, K.C., Pruszak, J., Yoshizaki, T., van Arensbergen, J., Sanchez-Pernaute, R., and Isacson, O. (2007). Enhanced yield of neuroepithelial precursors and midbrain-like dopaminergic neurons from human embryonic stem cells using the bone morphogenic protein antagonist noggin. Stem Cells *25*, 411–418.

Strömberg, I., Almqvist, P., Bygdeman, M., Finger, T.E., Gerhardt, G., Granholm, A.C., Mahalik, T.J., Seiger, A., Olson, L., and Hoffer, B. (1989). Human fetal mesencephalic tissue grafted to dopamine-denervated striatum of athymic rats: light- and electron-microscopical histochemistry and in vivo chronoamperometric studies. J. Neurosci. *9*, 614–624.

Swistowski, A., Peng, J., Han, Y., Swistowska, A.M., Rao, M.S., and Zeng, X. (2009). Xeno-free defined conditions for culture of human embryonic stem cells, neural stem cells and dopaminergic neurons derived from them. PLoS ONE *4*, e6233.

Thomson, J.A., Itskovitz-Eldor, J., Shapiro, S.S., Waknitz, M.A., Swiergiel, J.J., Marshall, V.S., and Jones, J.M. (1998). Embryonic stem cell lines derived from human blastocysts. Science *282*, 1145–1147.

Thompson, L., Barraud, P., Andersson, E., Kirik, D., and Björklund, A. (2005). Identification of dopaminergic neurons of nigral and ventral tegmental area subtypes in grafts of fetal ventral mesencephalon based on cell morphology, protein expression, and efferent projections. J. Neurosci. *25*, 6467–6477.

Ulloa, F., and Martí, E. (2010). Wnt won the war: antagonistic role of Wnt over Shh controls dorso-ventral patterning of the vertebrate neural tube. Dev. Dyn. *239*, 69–76.

Wictorin, K., Brundin, P., Gustavii, B., Lindvall, O., and Björklund, A. (1990). Reformation of long axon pathways in adult rat central nervous system by human forebrain neuroblasts. Nature *347*, 556–558.

Wictorin, K., Brundin, P., Sauer, H., Lindvall, O., and Björklund, A. (1992). Long distance directed axonal growth from human dopaminergic mesencephalic neuroblasts implanted along the nigrostriatal pathway in 6-hydroxydopamine lesioned adult rats. J. Comp. Neurol. *323*, 475–494.

Zuddas, A., Corsini, G.U., Barker, J.L., Kopin, I.J., and Di Porzio, U. (1991). Specific reinnervation of lesioned mouse striatum by grafted mesencephalic dopaminergic neurons. Eur. J. Neurosci. *3*, 72–85.